Experimental characterization of the thermo-electro-mechanical properties of a shape memory composite during electric activation

ClaraPereira Sánchez[1], Maxime Houbben[2], Jean-Francois Fagnard[1], Pascal Harmeling[1], Christine Jérôme[2], Ludovic Noels[3] and Philippe Vanderbemden[1]

[1] Department of Electrical Engineering and Computer Science, University of Liège, Liège, Belgium
[2] CERM, CESAM-RU, University of Liège, Liège, Belgium
[3] Department of Aerospace and Mechanical Engineering, University of Liège, Liège, Belgium

E-mail: capereira@uliege.be

Abstract

This works investigates in detail the electro-thermo-mechanical properties of a Shape Memory Composite (SMC) during shape memory cycles in which the heating is a result of resistive heating. The SMC is a covalently cross-linked poly(ε-caprolactone) network filled with 3 wt% of multiwall carbon nanotubes. The characterization is performed with the help of a custom-made tensile test bench that is able to couple the mechanical characterization with the thermal and electrical ones. A PI (Proportional Integral) controller using the lambda tuning method is used in order to control the temperature achieved by resistive heating of the SMC. The electrical resistivity of the SMC shows a non-linear and non-monotonic dependence on temperature and strain. The resistivity is also found to vary among successive shape memory cycles, suggesting that a (first) training cycle is necessary not only to stabilize the mechanical but also the electrical properties of the SMC. A fuzzy logic controller for constant load control is also used to investigate the strain variation with temperature related to the two-way shape memory effect of the SMC. The results give evidence of the strong interplay between the electrical and (thermo-)mechanical characteristics of electroactive SMCs.

Keywords: shape-memory, two-way shape memory, composites, carbon nanotubes, resistive heating, electroactivation

1. Introduction

Electroactive polymeric shape memory composites (SMCs) have been gaining interest in the past few years in research and various industrial fields [1-10]. They consist of a shape memory polymer (SMP) matrix in which an electrically conductive filler is dispersed. A conventional one-way shape memory (1W-SM) cycle of SMPs is accomplished by heating up the material above its transition temperature [11] and deforming it from the permanent to a temporary shape. The temporary shape can be fixed by cooling down at constant deformation the material below its transition temperature. Re-heating at zero load past its transition temperature leads to shape recovery, i.e. return to the permanent shape. Semi-crystalline SMPs can also undergo two-way shape memory effect (2W-SM) cycles [12]. These are achieved by heating above the transition temperature and deforming the SMC from the permanent to a primary temporary shape. If a constant load is kept, the SMC will go from the primary temporary shape to a secondary by cooling down below the transition temperature, i.e. with cooling, the SMC elongates in the loading direction during crystallization. The primary temporary shape can be recovered by re-heating up above the transition temperature, i.e. the SMC contracts in the loading direction with heating. The back-and-forth conversion between the secondary and the primary temporary shapes can be performed many times by repeating the cooling and heating steps at constant load.

Unlike conventional SMCs where heating and shape recovery is triggered with heating produced by an external heater, electroactive SMCs take advantage of resistive heating

within the material itself [3]. In order to achieve electroactivation, the electrical conductivity of the shape memory polymer needs to be high enough. To that end, conductive fillers such as carbon nanotubes [13, 14], carbon black [9, 15], graphene [16] or metallic nanoparticles [17] are dispersed into the polymeric matrix.

In the electroactivation process, the amount of heat generated within the SMC depends on the electrical current being injected, its geometry and its electrical resistivity ρ_e. The resistivity of an electroactive SMC has already been reported to vary with filler content [18, 19] or temperature [2, 8], among others. There are, however, very few reports on the strain dependence of ρ_e, [5, 19-21]. In addition, the monitoring of the electrical properties of the SMC during a full shape memory cycle has, to our knowledge, not yet been covered in spite of its crucial importance for accurately and efficiently controlling the resistive heating of the SMC. Even though extensive investigations on the thermomechanical properties of shape memory polymers and composites are available [22-24], together with reports of the strain dependence in the loading direction with temperature during conventionally-heated 2W-SM cycles [25-27], no work has been found quantifying such values for an electrically triggered 2W-SM effect of an SMC simultaneously in both the loading and transverse directions. For the reasons mentioned hereinabove, simultaneous monitoring of strain, stress, temperature and electrical resistivity is carried out in the present work to better understand the interplay between the mechanical, electrical and thermal properties of such SMC during an electric activation process.

The experimental research described in the present paper consists on the detailed thermo-electro-mechanical characterization of a nanocomposite exhibiting shape memory properties and activated by means of an electric current. The SMC is chemically cross-linked poly(ε-caprolactone) (PCL) filled with 3 wt% of multiwall carbon nanotubes (MWCNTs). MWCNTs are chosen amidst other electrically conductive fillers due to their superior electrical and thermal properties while having low density and high aspect ratio. This facilitates the creation of an electrically conductive network inside of the composite with rather small filler concentrations. The presence of the fillers, therefore, has only a limited impact on the mechanical properties. Other fillers may be used to improve the electrical conductivity of PCL such as carbon nano-fibers [28], Au nanoparticles [29] and even graphene-MWCNT hybrids [30, 31]. When used at concentrations of around 3 wt%, the latter exhibits a range of values comparable to those found in the present work.

A bespoke tensile test bench, whose characteristics are described in section 2.4, was built in order to accommodate the extra features needed for the thermo-electro-mechanical characterization. Using this bench, the evolution of the electrical resistivity ρ_e is measured during three consecutive shape memory cycles. The shape memory properties of the SMC, such as the recovery stress, shape recovery ratio or shape fixity, are also investigated during electric activation. Further constant load control is also made possible using a

fuzzy logic controller; this enables to measure the 2W-SM characteristics of the SMC under a constant load.

2. Experimental methods

2.1. Processing of the material

The material used in this study is made by end-groups functionalization of commercially available star-shaped PCL samples (CAPA™ 4801, Perstorp®) following the procedure reported in [32]. The composite is prepared by grinding together in a mortar stoichiometric amounts in reactive groups (furan and maleimide moieties) of PCL76-4MAL (functionalized with maleimide end-groups) and PCL76-4FUR (functionalized with furan-end groups) powders and then mixed with 3 wt% of MWCNTs (Nanocyl 7000, properties given in Appendix A). The mixture is then melt-blended at 105 ℃ in a 6 cm^3 co-rotating twin screw mini-extruder (Xplore, DSM) for 60 min at 150 rpm. The polymer blend is then pressed at 105 ℃ to a flat sheet of 0.5 mm at a load of 75 N for 90 s and then let to cool down to room temperature. A post-curing is performed for 3 days at 65 ℃ in a ventilated oven under load. Transmission Electron Microscopy (TEM) images (available in Appendix B) are used to visually validate the MWCNT dispersion within the SMP matrix. The filler concentration was determined during preliminary experiments. A concentration of 3 wt% is chosen in the present study for two reasons (refer to Appendix C): (i) a better reproducibility of electrical properties during electrically activated shape memory cycles, and (ii) to ensure a well-connected electrical network within the SMC during the elongation of the samples.

Differential scanning calorimetry (TA Instruments DSC 250) was performed on the (unloaded) SMC samples with heating and cooling ramps at ±10 ℃·min^{-1} between 25 and 65 °C. The DSC curve, given in Appendix D, shows that the SMC starts melting at $T_{m,0}$ = 28.6 °C and ends at $T_{m,f}$ = 52.7 ℃. The peak melting temperature (T_m) is 43 ℃. The SMC has a crystallinity degree of 31.1%. During cooling crystallization starts at T_{C1} 36.9 °C and finishes after 5 min of isotherm at 25 °C.

2.2. Measurement of the temperature

The temperature is measured on the surface of the sample in a contactless fashion with a thermal infrared camera (COX CX320) that has been previously calibrated in-house. In order to obtain an accurate temperature measurement (± 1 ℃) the readings from the IR camera are corrected for the finite emissivity of the samples, which is measured to be 0.91 ± 0.03. The temperature on the surface is recorded during the full shape memory cycle and given as input to the temperature control loop system.

2.3. Measurement of electrical properties and resistive heating

Rectangular samples of 41 by 8 mm are cut from the 0.5 mm thick SMC sheet. The samples are cleaned with isopropanol

before painting four electrodes with silver paste (Agar scientific, Electrodag 1415). Thin wire leads are placed in the electrodes to enable the measurement of the electric resistance in a four-point measurement configuration. A Keithley 2400 source meter is used to inject an electric current through the samples. The voltage across them is measured using a Keithley 2100 voltmeter and the resistance of the samples is calculated. Importantly, the resistance is converted to ρ_e by using the instantaneous dimensions of the samples, i.e. taking into consideration the strain measured in the parallel and perpendicular directions to the applied deformation (see section 2.4).
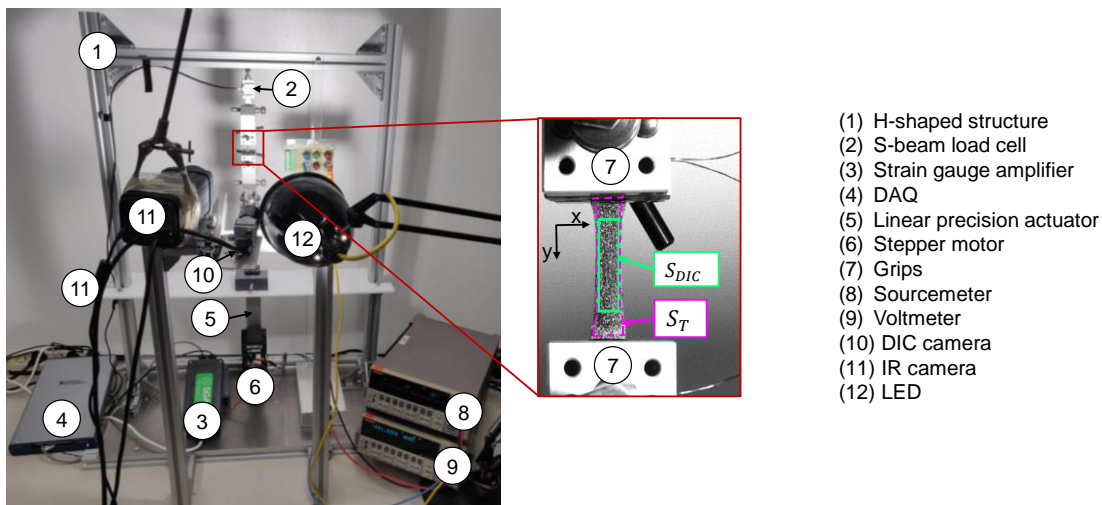
Regarding the value of the injected current, two situations can arise: (i) the injected current is required to achieve a well-defined resistive heating; the value is therefore set by the control loop described in Section 2.5 below, or (ii) no resistive heating is needed; the injected current is set to the lowest possible value (0.5 mA), at which no measurable resistive heating occurs. The measurement of resistance, therefore, is still carried out during all steps of the shape memory cycle.

2.4. Measurement of mechanical properties

A bespoke tensile test bench was fabricated for the measurement of the mechanical properties of the SMC, it is shown in Figure 1. Besides the measurement of force and strain, this tensile test bench includes additional features that enable temperature control by electroactivation. The structure of the tensile test machine is made of an aluminum plate onto which an H-shaped structure (1) is fixed, standing vertically.

The H-shaped structure is made with Bosch Rexroth ® strut profiles (cross-section 30×30 mm) cut to length by the manufacturer. The brackets and connectors are all selected within the same brand for optimal assembly at right angles and force transmission. A S-beam load cell (2) from Applied Measurements (DBBSMM-2kg) is fixed on its upper end to the center of the horizontal strut. The load cell is connected to (3) a strain gauge amplifier (Applied Measurements, SGA/A). The load cell system is calibrated by the manufacturer. In order to measure the force, the strain gauge amplifier is connected to (4) a data acquisition system (DAQ NI, USB-6341) connected to a computer running LabVIEW.

The moving part of the tensile test bench, in charge of setting the elongation of the sample, is located below the load cell, on its same vertical axis. It is composed of (5) a linear precision actuator (Thomson, PC25) driven by (6) a stepper motor (Moons' TSM23Q-3RG), which is powered by a 48 VDC power supply (Mean Well, HRP-300-48). The actuator system is controlled in LabVIEW for a specified vertical displacement at a specified linear vertical speed, i.e. the motion happens in the y-direction. Two grips (7) are used in the tensile test bench in order to elongate the SMC samples: the mobile one is located on top of the linear actuator and the fixed one is attached on the lower end of the load cell. The grips are vise U-shaped (AML Instruments, TH240k) with stainless steel jaws covered with rubber (AML Instruments, TH240k-BG-A4) to electrically insulate the SMC from the tensile test bench. A series of clevises are used in order to ensure the alignment of the grips when attached to the sample.

(1) H-shaped structure
(2) S-beam load cell
(3) Strain gauge amplifier
(4) DAQ
(5) Linear precision actuator
(6) Stepper motor
(7) Grips
(8) Sourcemeter
(9) Voltmeter
(10) DIC camera
(11) IR camera
(12) LED

Figure 1: Experimental set-up of the bespoke tensile test bench for the electro-thermo-mechanical characterization of shape memory composites.

The SMC samples are held vertically in between the grips. The printed circuit board (PCB) located on the right of the samples is used to connect the thin wire leads from the sample to (8) the precision sourcemeter (Keithley 2400) and (9) voltmeter (Keithley 2100). Directly facing the sample, a high-speed camera (10) (Basler, acA2040-120um with Edmund Optics 8.5 mm C series lens) records the visible surface of the sample, i.e. in the xy-plane. The images are saved and fed to a

Digital Image Correlation (DIC) open access software (ncorr) for post-processing in order to obtain the 2D Green-Lagrangian strain field $\varepsilon_{GL}(x, y)$. The region of interest for DIC is set away from the grips in the central area of the sample (S_{DIC}, delimited in green in Figure 1). The speckle pattern required for DIC is obtained by spraying white paint (MoTip Carat matt white) on the surface of the samples. An infrared (IR) camera (11) is used to measure the surface temperature of

the sample (region delimited in dashed pink in Figure 1). A 60 W 4500 K LED light (12) for good illumination of the sample is located on the side of the DIC camera system.

The stress-strain curves obtained with this bespoke tensile test bench were compared to calibrated commercially-available universal testing machines (Instron 5566 and Zwick Z100) on Teflon and pristine PCL samples; a maximum disagreement of <1.5 % was observed.

In this work, the reported strain is the surface average of the Green-Lagrange (GL) strain in the loading direction $\varepsilon_{y,GL}$ in the area S_{DIC} (see Figure 1). Most experimental investigations on SMC report the classical engineering stress (i.e. considering the initial dimensions of the sample) since this is the stress provided by the loading machine. In this investigation, the reported stress is the average true stress, which takes into consideration the instantaneous $\varepsilon_{y,GL}$, $\varepsilon_{z,GL}$ and $\varepsilon_{x,GL}$ and hence is closer to the real stress experienced by the material. $\varepsilon_{x,GL}$ is the average (along y) of the instantaneous strain in the transverse direction (x-direction) measured at the faces normal to x. Similarly, $\varepsilon_{z,GL}$ is the strain in the through-thickness direction (z-direction), which is assumed to be equal to $\varepsilon_{x,GL}$ at any given instant. Furthermore, unless otherwise stated, the reported electrical resistivity ρ_e takes into consideration the instantaneous dimensions of the sample calculated from $\varepsilon_{x,GL}$, $\varepsilon_{y,GL}$ and $\varepsilon_{z,GL}$.

2.5. Temperature control of resistive heating

In a shape memory experiment, the temperature of the sample is usually controlled either to be at a constant temperature T, or a ramp at a constant rate dT/dt. For the experiments described in this work, temperature control is achieved by resistive heating of the SMC. In all parts of the sample subjected to a local current density J, the local dissipated power is given by $\rho_e J^2$. One practical issue is that the resistivity ρ_e changes continuously during the experiment: ρ_e has already been reported to be dependent on the local temperature of the SMC 33] and on strain [5]. In our experiments, a dedicated PI temperature control loop is implemented in LabVIEW with the following goals: (i) to control the heating ramp to avoid too sudden local hot-spots that could damage the samples and improve the temperature uniformity throughout the sample, (ii) to control the cooling ramp so that the crystallinity of the polymer matrix is nearly the same before and after each shape memory cycle, (iii) to achieve a constant temperature above the transition temperature of the polymer even if the resistivity of the sample varies due to deformation or shape recovery. The input signals to the controller are the average measured temperature on the surface of the SMC, the temperature set-point and the output is the electric current injected to the sample using the Keithley 2400 sourcemeter.

Resistive heating is a fast occurring phenomenon where the heat flux is generated within the material itself upon the injection of an electric current. The open loop response of the system can therefore be approximated to that of a first order system with no dead time, whose transfer function in the frequency domain $G(s)$ is recalled in equation (1), where K and τ are the process gain and time constant respectively.

$$G(s) = \frac{K}{\tau s + 1} \qquad (1)$$

Most common PI (Proportional Integral) and PID (Proportional Integral Derivative) tuning techniques such as Ziegler-Nichols, Cohen-Coon or Chien-Hrones-Reswick [34-36] rely on the knowledge of a finite dead time to compute the PI or PID gains, and thus cannot be applied for resistive heating. In the present case, the lambda tuning method [37] is used, which is a form of the Internal Controller Method (ICM) for a PI controller. For a first order system with no dead time, the method is characterized by one tuning parameter (λ) which allows the user to choose the PI parameters. If the controller action $u(t)$ is defined as $u(t) = K_c \left(e(t) + \frac{1}{T_i} \int_0^t e(t)\, dt \right)$, where e is the error (difference between desired temperature and measured temperature), both the controller gain (K_c) and the integral time (T_i) can be found using equation (2) and (3).

$$K_c = \frac{\tau}{K\lambda} \qquad (2)$$

$$T_i = \tau \qquad (3)$$

This tuning method can be applied either after a preliminary open-loop test used to find K and τ, or integrated in the LabVIEW program using the "PID Autotuning VI" with equivalent results. For the experiments described in this work, a λ of 0.46 min is used. Figure 2(a) shows the controlled temperature vs. time on a SMC upon a temperature cycle composed of heating up to 60 °C at 10 °C·min⁻¹, isotherm at 60 °C and cooling at - 10 °C·min⁻¹ to room temperature. The temperature set-point T_{SP} is shown in dashed red and the measured temperature in a solid black line. As can be seen, the controller provides an excellent control of temperature during the heating and isotherm parts of the cycle, with a maximum deviation < 0.8 °C. During cooling, when the temperature gets close to room temperature (i.e. $T < 30$ °C), the cooling stops being dictated by the controller (i.e. injected current is set to the minimum 0.5 mA) and natural convection takes place, rendering the temperature ramp slower than the prescribed set-point. These results evidence that the lambda tuning method provides an adequate temperature control during heating, constant temperature and most of the cooling process. For additional information, Appendix E explains the importance of a temperature controller and shows the time evolution of the required injected current to obtain such temperature treatment and the measurement of resistivity of the sample.

2.6. Constant load control in the tensile test bench

Tensile tests are conventionally performed either by controlling the load (and measuring the displacement) or controlling the displacement (and measuring the load). For the 1W-SM cycles in this investigation, the tensile test bench is operated in "controlled displacement", which can be achieved easily using the linear actuator (see section 2.4). For other applications, however, a bench operated in "controlled load"

is desirable. In our tensile test bench, a load controller was implemented in order to investigate the temperature dependence on strain at zero or non-zero constant load, that is characteristic of 2W-SM composites. The actuator/grip mechanism adjusts the position of the lower grip in order to maintain a constant load on the sample. The time-dependent position cannot serve as controlled variable because the integrated controller of the stepper motor driving actuator does not overwrite the commands and, instead, chains them in a first-in-first-out fashion. The parameter that can be changed while in operation is the rotational velocity: positive (grip going up), negative (grip going down) or zero (stationary grip). This, together with the fact that the mechanical properties have a non-linear dependence with temperature [7, 38], makes conventional PIDs not suitable for this controller. Although robust and efficient, intelligent adaptive PID controllers based, e.g. on fuzzy logic or neural networks [39, 40] are usually memory heavy and will not be considered due to the large amount of data that needs to be collected and processed simultaneously (i.e. images used for DIC and temperature control). In the present work, it was found that a very efficient way to achieve load control is to implement directly a fuzzy logic controller based on the load error

(difference between the measured load and the constant load set-point) used as an input variable. The controller then calculates the corresponding actuator linear velocity. More information about the designed controller is available in appendix F. Figure 2(b) shows the load vs. time achieved during a heating ramp for one min directly followed by a cooling ramp. A reduced temperature interval is shown here for clarity in order to obtain a smaller load scale and be able to distinguish the small variations of the controlled load. This temperature treatment was run twice in order to measure (i) the non-controlled load (in grey) that arises due to the elongation/contraction of the sample with fixed grips and (ii) the controlled load (in black) that is a result of the grip position adjustments made thanks to the fuzzy logic controller with a constant load set-point shown in dashed red. The load error is < 1.2% whereas, if no controller is used, the difference between the initial and the measured minimum load would be of 15.9%. These results give evidence that the fuzzy logic controller relying on the load error provides a very satisfactory constant load control of the tensile test bench for the investigation of the 2W-SM characteristics of the SMC.
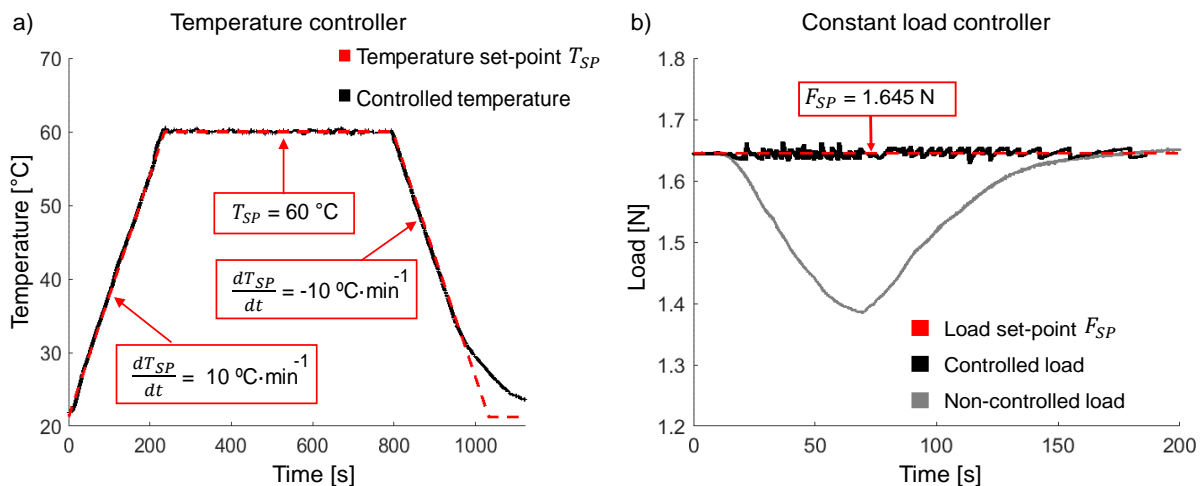
Figure 2: Result of the control loops for (a) temperature PI controller tuned using the lambda tuning and (b) constant load fuzzy logic controller. The set-point (a) temperature and (b) load values are shown in dashed red lines. The measured controlled (a) temperature and (b) load are given in solid black lines. The controlled load is measured during the temperature cycle shown in dashed blue (to be read in the secondary *y*-axis). For comparison, (b) shows the non-controlled load in solid grey that is obtained upon the same temperature cycle.

2.7. Description of the tests performed to the SMC

2.7.1. Thermal reset treatment. Prior to any shape memory test, a thermal reset treatment is performed on the samples in order to have similar crystallinity at each instance. It consists of heating up the sample up to 60 °C at 10 °C·min^{-1}, stabilizing at 60 °C for 5 min and cooling down to room temperature at -10 °C·min^{-1}. This is done by resistive heating. The sample is left at room temperature for 10 additional minutes prior to the start of the shape memory test run.

2.7.2. One-way shape memory (1W-SM) test cycle. The sample is fixed in between the grips of the tensile test bench. The shape memory test cycle, sketched in Figure 3, can be divided into 6 different steps:

1 – Heating: starting from the permanent shape, the material is heated from room temperature to 60 °C thanks to resistive heating. The heating ramp is controlled to be 10 °C·min^{-1}. The sample is left at 60 °C for 5 min. No stress is applied to the sample during this step.

2 – Loading: the sample is elongated to the temporary shape while maintaining the temperature at 60 °C. Elongation amounts to 100% the original length in between the grips. The strain rate is set to 0.02 mm·s^{-1}.

3 – Shape fixity: the sample is cooled down to room temperature at -10 °C·min^{-1} at constant strain. The sample is left at room temperature for 10 min to ensure full crystallization.

4 – Constrained heating: the sample is heated from room temperature to 60 ℃ at 10 ℃·min⁻¹ at constant strain. The recovery stress is measured during this step. The sample is left at 60 ℃ for 5 min.

5 – Constrained cooling: similar to step 3.

6 – Shape recovery: the lower grip of the tensile test bench is removed and the sample is left free on its lower side. The sample is heated from room temperature to 60 ℃ at 10 ℃·min⁻¹. The sample is left at 60 ℃ for 5 min. The recovery ratio is measured at the end of this step.
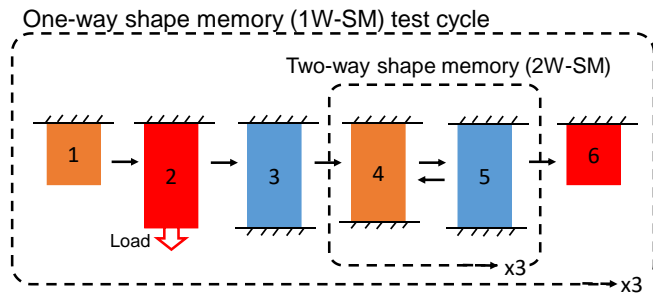
Figure 3: Sketch of a cycle of one-way shape memory (1W-SM) test: 1 – Heating, 2 – Loading, 3 – Shape fixity, 4 – Constrained heating, 5 – Constrained cooling and 6 – Shape recovery. The full shape memory test cycle is repeated 3 times and within each cycle, the constraint shape recovery is repeated 3 times. For clarity, 1W-SM cycles will be referred from now on as "cycles" and each 2W-SM run will be noted as "run".

In order to assess the repeatability and potential wearing consequences, three consecutive 2W-SM runs are performed per 1W-SM test cycle (i.e. steps 4 and 5 are repeated three times). The complete 1W-SM cycle is also redone three times in order to check how the properties of the SMC are affected by the shape memory cycles. Additionally, to evaluate the quality of the shape memory behavior of the SMC, we look at the commonly used shape fixity ratio (R_F) and shape recovery ratio (R_R). Their definitions are given in equations (4) and (5) respectively. R_F is defined as the ratio of the strain in the stress-free configuration (i.e. strain at the start of step 6 after the grip is removed, $\varepsilon_{6,initial}$) to the maximum strain after deformation (i.e. strain at the end of step 2, $\varepsilon_{2,final}$). Conversely, R_R is defined as the ratio between the difference in strain of step 6 to the difference between the strain at end of Constrained cooling ($\varepsilon_{5,final}$) and at the end of Heating ($\varepsilon_{1,final}$).

$$R_F = \frac{\varepsilon_{6,initial}}{\varepsilon_{2,final}} \times 100\ \% \qquad (4)$$

$$R_R = \frac{\varepsilon_{6,initial} - \varepsilon_{6,final}}{\varepsilon_{5,final} - \varepsilon_{1,final}} \times 100\ \% \qquad (5)$$

2.7.3. Two-way shape memory (2W-SM) test cycle. Since the temperature dependence of strain during a 2W-SM cycle ($\varepsilon_{T,2W}$) depends on the load being exerted on the material [25], it is of interest to be able to maintain and perform the investigation at different constant loads. In order

to achieve so, the sample is heated up to 60 ℃ at 10 ℃·min⁻¹ and zero stress, and after stabilizing the temperature for 5 min, the grip/actuator mechanism will deform the sample until the desired load is obtained. The constant load control option in section 2.6 is then activated. The sample is cooled down to room temperature at -10 ℃·min⁻¹ while maintaining a constant load and left at room temperature for 10 min to fully crystallize.

For a zero constant load, the strain variation with temperature can be used to approximate the linear coefficient of thermal expansion (CTE) assuming linearity over a temperature range.

If a non-zero load is applied above the melting point of the material, crystallization results in the elongation of the sample when cooling and contraction when heating. The measurement of $\varepsilon_{T,2W}$ due to the 2W-SM effect starts by re-heating the sample to 60 ℃ at the usual controlled 10 ℃·min⁻¹, keeping the desired constant load. Meanwhile, the image acquisition system captures images that will be fed to the DIC code to measure the 2D strain field of the sample while heating. Once at 60 ℃ and after stabilizing the temperature for 5 min, the same measurement procedure is followed during cooling.

3. Results and discussion

3.1. Electrical resistivity during the one-way shape memory (1W-SM) test cycle

The evolution of electrical resistivity ρ_e during the first four steps of the 1W-SM cycles is shown in Figure 4. During step 1, the temperature increases from room temperature to 60 ℃. The ρ_e of the SMC shows a non-monotonic evolution during the heating process (Figure 4(a), step 1): it rises with T until almost the peak melting temperature T_m (grey dot in Figure 4(a)) of the SMC is reached and decreases past it. The injected current grows from 0.6 mA to 15.7 mA for the reported sample during this step. During step 2 the sample is deformed at a constant strain rate and temperature ($T = 60$ ℃). Figure 4(b) shows that, initially, ρ_e decreases with applied strain. This phenomenon is likely due to the aided alignment of the MWCNTs in the direction of elongation [41], which also corresponds to the direction in which ρ_e is measured. After a certain strain level, referred hereinafter as critical strain, ε_c (marked with crosses in Figure 4(b)), ρ_e starts increasing even though the cross section of the sample (shown in dashed lines to be read on the secondary y-axis) decreases with applied strain in the loading direction. A possible cause for the increment in ρ_e is the deformation of the SMC matrix itself, increasing the average distance between MWCNTs. Even though the SMC has been stretched, it is worth noting that the ρ_e always remains on the same order of magnitude, since 3 wt% MWCNT is well above the percolation threshold. The injected current starts at 15.7 mA and ends at 10.9 mA for the reported sample during this step. The high final values of ε_{GL} are explained by the necking experienced by the sample: most of the deformation happens in the surface area S_{DIC}, while

little to no deformation happens in the areas of the sample closer to the grips. This means that, for a total applied strain of 1 mm·mm^{-1}, the average of the strain in S_{DIC} is >1 mm·mm^{-1}. Moreover, the reported strain is ε_{GL} along the loading direction, which relates to the applied engineering ε_{eng} strain by: $\varepsilon_{GL} = \frac{1}{2}\left((\varepsilon_{eng} + 1)^2 - 1\right)$. Furthermore, it is interesting to mention that the final value of ρ_e after

deforming the sample is 8% smaller than at the beginning of Step 2 for cycle 1, and around 21% for cycles 2 and 3. It appears that, although the elongation may place the MWCNT further once past ε_c, the assisted alignment in the direction of the elongation is strong enough to globally counteract this effect during Step 2 for the levels of applied strain investigated here.
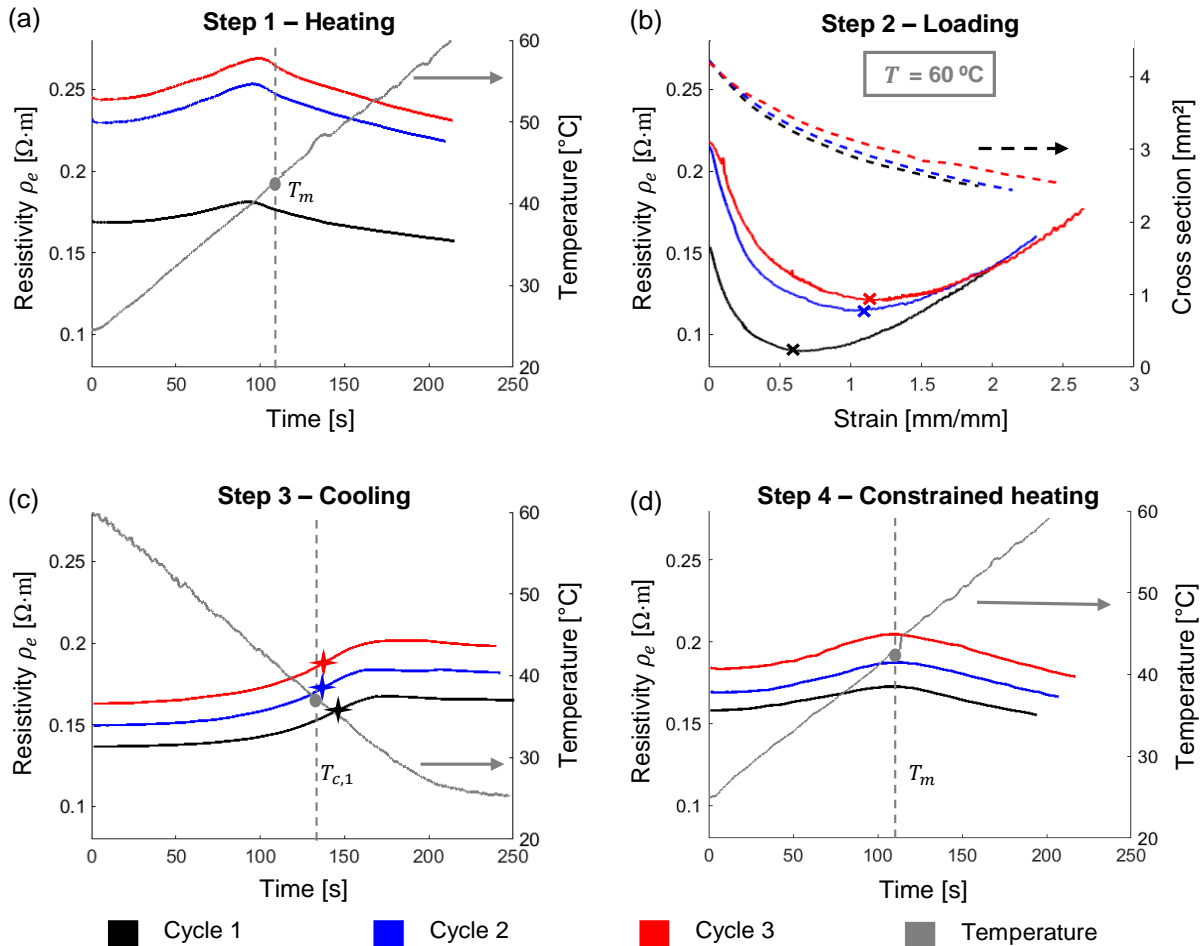
Figure 4: Evolution of resistivity during (a) step 1 – Heating, (b) step 2 – Loading, (c) step 3 – Cooling and (d) step 4 – Constrained heating. The first three shape memory test cycles performed on a SMC sample are shown: the first in black, second in blue and third in red. The temperature, whenever plotted, is shown in grey and should be read on the secondary *y*-axis. The cross section evolution with strain during loading is shown in dashed lines in (b) and should be read on the secondary *y*-axis. A grey dot specifies the start of crystallization $T_{c,1}$ in (c) and the melting temperature T_m in (a) and (d). In (b) crosses mark the critical strain ε_c. In (c) stars mark the maximum slope.

After the deformation, the sample is cooled down at room temperature (step 3) to fix the temporary shape. The resistivity ρ_e during this step shows a prolonged increase. The maximum slope of the $\rho_e(T)$ dependence (denoted with stars in Figure 4(c)) is found to coincide with the start of crystallization $T_{c,1}$ = 36.9 °C (shown as a grey dot in Figure 4(c)) within 2.2 °C for the first cycle and within 0.2 °C for the second and third cycles. One possible explanation is that during crystallization the polymer expands in the direction of loading. The MWCNTs, located only in the amorphous part of the PCL, may then be pushed further apart from each other. Furthermore, the crystals within the SMC align with the

direction of the applied elongation. This oriented crystallization reinforces the alignment of the MWCNTs, increasing the separation among them and breaking the current path. Both of these effects result in an increase of ρ_e. The injected current decreases from 11.0 mA to 0.6 mA for the reported sample during this step. Finally, Constrained heating (step 4) is investigated. Note that for each cycle, the constrained shape recovery is run 3 times (see Figure 3). Only the first run is shown in Figure 4(d) for clarity (the comparison among the 3 runs will be done in Figure 5). When the sample is re-heated to 60 °C, ρ_e shows a similar trend to that of step 1, although at lower average values for each cycle due to the overall decrease of resistivity in Steps 1 and 2.

When comparing the three different cycles presented in Figure 4, ρ_e shows an obvious increase between cycle 1 and 2 during Steps 1 and 2. Nevertheless, after Step 2 of the first cycle, the variation of ρ_e between consecutive cycles (within each step) seems to have stabilized to $< 8\%$, instead of the maximum 40% difference between cycle 1 and 2 in Step 1. These results give evidence that the SMC needs training in order to stabilize, not only its mechanical properties (as reported e.g. in ref. [42]), but also its electrical resistivity. This has practical consequences on the resistive heating, that depend on how the amplitude of the injected current is chosen. Three situations can be considered. (i) If a constant current I_0 is used, the change in resistivity depicted in Figure 4 yields a change of the total resistance R that strongly affects the dissipated power RI_0^2, so this configuration should be avoided. (ii) If the current is regulated so that the total power RI^2 is constant, our previous work [33] showed that the temperature dependence of the resistivity still affects the final temperature, mainly because the temperature distribution within the sample cross-section is not uniform. (iii) In this work, the current value is constantly adjusted through the PI controller with parameters chosen with the lambda tuning. The results shown in Figure 4 give further evidence that an adequate temperature control is achieved despite the resistivity variation with time.

The comparison among the three runs of the constrained shape recovery for the first cycle is shown in Figure 5 (see appendix G for cycles 2 and 3). Figures 5(a) and (b) respectively show steps 4 and 5. The evolution of ρ_e with temperature shown during constrained shape recovery is as expected for either a heating or a cooling ramp, i.e. qualitatively similar evolutions than steps 1 and 3 respectively. Nonetheless, within each cycle, ρ_e decreases after each run of constrained shape recovery. A possible explanation for this phenomenon is that the MWCNTs move during every cycle, causing further stacking and consequently more electrical contacts within the SMC network.

Lastly, Figure 6 shows the evolution of the electrical resistivity $\rho_{e,0}$ during step 6 – Shape recovery, for the three cycles together with their temperature evolution with time. It should be noted that, during shape recovery, the shape of the sample changes quickly due to the melting of the crystalline regions. Because not all crystalline regions are molten at the same time, the sample momentarily bends in different directions until melting is completed and the initial shape is reached. The strain measurement is therefore not possible when the sample deforms out-of-plane. Since the instantaneous dimensions of the sample cannot be accurately determined, ρ_e is calculated using the original dimensions of the sample at the start of each cycle (beginning of Step 1), hence the notation $\rho_{e,0}$. Looking at Figure 6, $\rho_{e,0}$ shows the same evolution as in the previous heating steps: it increases with temperature up to T_m and decreases past it. However, the difference of the maximum $\rho_{e,0}$ with respect to its value at the beginning of the step is much bigger than in the previous heating steps (e.g. difference at step 1 was of 9, 10 and 11% for each cycle respectively, while during step 6 the difference amounts to 34, 54 and 47%). This difference would be even

bigger if the shrinkage of the sample due to shape recovery could be taken into consideration. During these instants of bending, the MWCNTs may be placed further apart from each other, provoking the increase of resistivity.

The set of measurements presented in this section 3.1 were also carried out on thicker samples (0.7 mm). Similar results were obtained, hence suggesting that the presented characteristics are not a result of a surface effect.
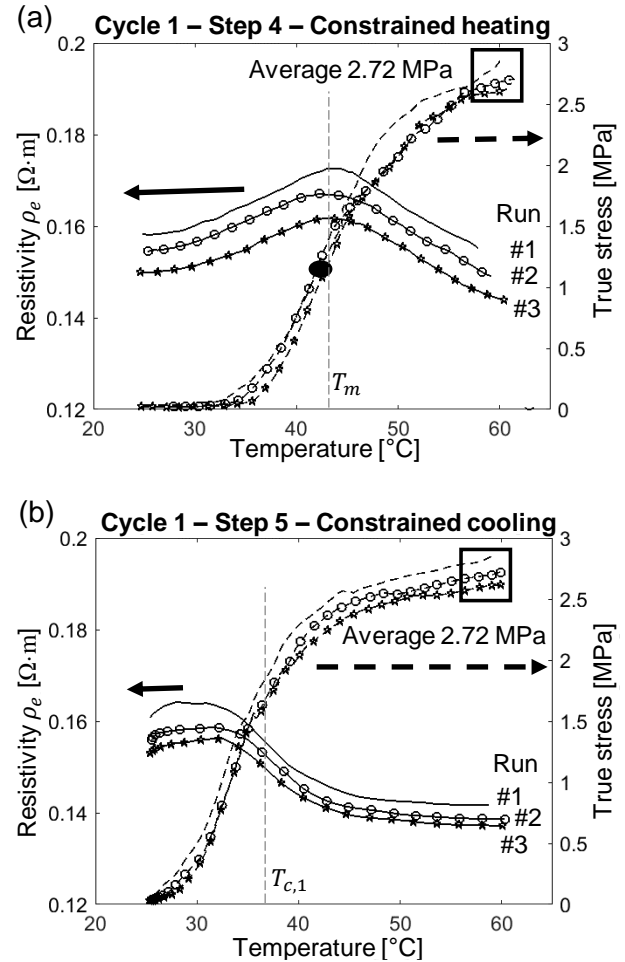
Figure 5: Temperature dependence of resistivity and stress measured during (a) step 4 – Constrained heating and (b) step 5 – Constrained cooling. Three consecutive runs are shown: run 1 (no marker), run 2 (circles) and run 3 (stars). Solid lines are used for resistivity and should be read on the primary y-axis. Dashed lines are used for the stress and should be read on the secondary y-axis. The solid dot in (a) marks the inflexion point of recovery stress vs. temperature. Grey vertical dashed lines mark (a) T_m and (b) T_{c1}.
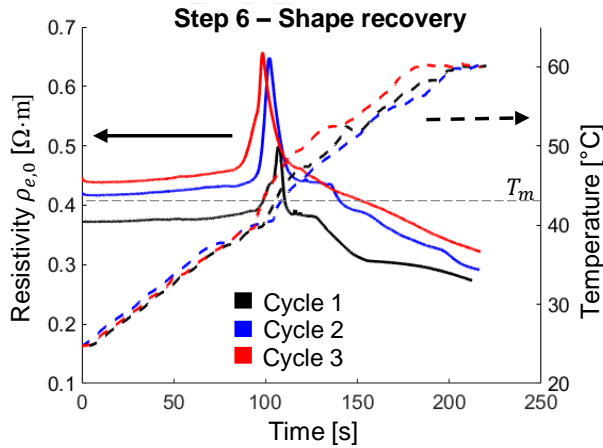
Figure 6: Electrical resistivity and temperature vs time during step 6 – Shape recovery. The resistivity is shown in solid lines and should be read on the left axis. Dashed lines show the temperature evolution with time and should be read on the right axis. Cycle 1 (black), cycle 2 (blue) and cycle 3 (red) are shown. Horizontal grey dashed line marks the melting temperature.

3.2. Mechanical properties during the one-way shape memory (1W-SM) test cycle

The stress vs. strain curve for the SMC during step 2 is shown in Figure 7 for the three investigated cycles. The corresponding Young's moduli E, calculated at the beginning of the curves, and Poisson's ratio ν_{xy} are given in Table 1. The SMC is shown to be is stiffer during the first shape memory cycle. Cycles 2 and 3 show a more familiar curve for ductile polymers [43], with strain softening and necking of the sample followed by strain hardening. All experimental stress-strain curves in Figure 7 are found to exhibit an inflexion point, which are marked with vertical arrows in Figure 7. They are located respectively at 0.47 (cycle 1) and at 1.21 GL strain (both cycles 2 and 3). On the same curves, the critical strains ε_c that were pointed out in Figure 4 step 2 are shown with crosses. Remarkably, the inflexion points in Figure 7 are extremely close to the values of ε_c observed from the electrical resistivity data. The data from Figure 7 seems to suggest that this critical strain ε_c is related to strain hardening; it then makes sense that ε_c increases from the first (training) to the second cycle and stays nearly constant afterwards.

During step 4, the average true recovery stress σ_R was also measured for the three runs. The results can be seen in Figure 5(a) as a function of time. It is of interest to point out that the sudden increase in σ_R, corresponding to an inflexion point marked with a solid dot, almost coincides with the peak in the ρ_e curve. This makes sense since both are related to the melting point of the SMC. Additionally, the final value of σ_R (when the SMC is at 60 ºC), whose average values are reported in Table 1 for the three cycles, is found to decrease with each shape memory cycle. This is because, as implied in Figure 7, a lower load is applied each cycle on the sample in order to achieve the specified elongation. During Constrained cooling, (Figure 5(b)), σ_R decreases when crystallizing down to < 0.05 MPa at room temperature. This happens because, when cooling, the (temporary) deformed shape gets fixed by the

newly formed crystals. The corresponding information in the subsequent cycles 2 and 3 are reported in appendix G.
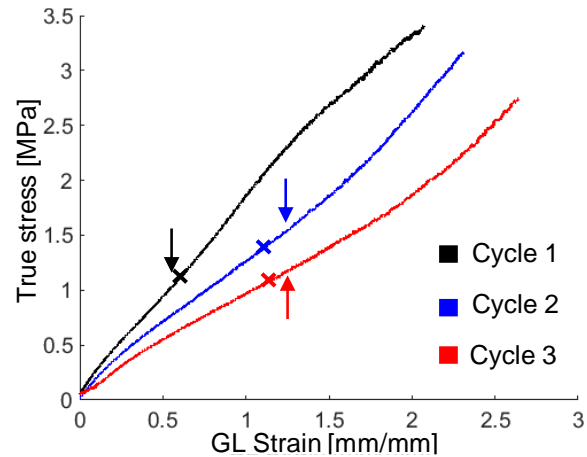
Figure 7: Stress-strain curves measured during loading (1W-SM). Cycles 1 (in black), 2 (in blue) and 3 (in red) are shown. The inflexion points at low strain are marked with vertical arrows. Crosses mark the critical strain ε_c values that were determined.

Table 1: Mechanical and shape memory properties of the SMC samples during the first three shape memory cycles.

	Cycle 1	Cycle 2	Cycle 3
E [MPa]	2.23	1.83	0.78
ν_{xy} [-]	0.26	0.23	0.21
$\sigma_R{}^*$ [MPa]	2.72	2.57	2.23
R_F [%]	98.2	98.1	96.9
R_R [%]	88.9	96.7	96.6

* Reported value of recovery stress is the average of the final value in each of the three runs of Constrained heating

The shape fixity and shape recovery ratio (R_F and R_R respectively) are also reported in Table 1. The shape fixity ratio R_F, even though always close to 100%, decreases with each cycle. The shape recovery ratio R_R of the first cycle is much lower than for the two following ones. Both of these observations can be explained by the fact that damage occurs within the material due to mechanical and thermal stress, causing the rupture of certain links within the composite matrix. For cycles 2 and 3, the recovery ratio is much closer to 100%, as is expected after the first cycle which serves to train the material.

3.3. Thermo-mechanical properties during the two-way shape memory (2W-SM) test cycle

Lastly, the 2W-SM characteristics of the SMC are investigated. The strain measured on the sample during a heating ramp at constant stress, is shown as a function of temperature in Figure 8 (see Appendix H for the complete heating and cooling cycle). The strain in the *x* and *y*-directions (transverse and loading directions respectively) at two stress levels of 0 and 600 kPa are shown. The stress is pre-applied at 60 °C in a previous temperature cycle (see section 2.7.3).

The estimation of the linear CTE during heating can be calculated for constant zero stress. Five temperature regions

are defined for this purpose based on the melting process of the SMC. It is recalled here that $T_{m,0}$ and $T_{m,f}$ are the initial and final temperature at which melting occurs, i.e. 28.6 and 52.7 °C respectively (see section 2.1) and T_m the peak melting temperature of 43 °C. The five temperature regions for the calculation of the CTE during heating are defined as follows:

(I) $T < T_{m,0}$; (II) $T_{m,0} < T < T_m - 2$ °C; (III) $T_m - 2$ °C $< T < T_m + 2$ °C; (IV) $T_m + 2$ °C $< T < T_{m,f}$; (V) $T_{m,f} < T$.

The CTE in the x and y-directions in each of these regions during heating is reported in Table 2. Similar regions are defined for the calculation of the CTE during cooling, which can be found in Appendix G. The CTE at 0 kPa is positive and small at all times ($<10^{-3}$ °C^{-1}). The slight difference between CTEx and CTEy may be due to the small pre-load required to straighten the sample after fixing it between the grips.
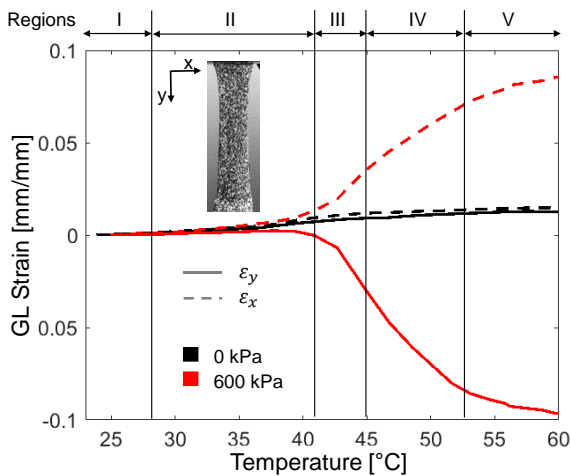
Figure 8: Evolution of GL strain during heating at constant stress for the investigation of the two-way shape memory (2W-SM) effect. Two constant stress levels are shown: 0 kPa in black and 600 kPa in red. The strain in the x-direction is shown dashed and the strain in the y-direction in solid line. Five regions are identified for the calculation of the CTE (at 0 kPa) during heating.

Table 2: Estimation of the Coefficient of Thermal Expansion at zero stress during heating in the loading and transverse direction (CTEy and CTEx respectively) in the five specified temperature regions.

Region	I	II	III	IV	V
CTEx [10^{-3} °C^{-1}]	0.3	0.7	0.3	0.2	0.2
CTEy [10^{-3} °C^{-1}]	0.2	0.5	0.5	0.4	< 0.1

At a higher pre-stress of 600 kPa and in regions I and II, the evolution of strain with temperature ($\varepsilon_{T,2W}$) in the x and y-directions does not experience a dramatic change with respect to that at 0 kPa. However, when approaching T_m and until $T_{m,f}$ (regions III and IV), the absolute value of $\varepsilon_{T,2W}$ is considerably higher than at 0 kPa. In region V, where most of the SMC is presumably molten, the absolute value of the $\varepsilon_{T,2W}$ in the x and y-directions at 600 kPa is still larger than that at no load, although the slope has decreased by >63% from that of region IV at 600 kPa. Furthermore, it can be noticed that, at 600 kPa, the absolute value of $\varepsilon_{T,2W}$ is highest for

temperatures around T_m (region III). This is because, besides the conventional effect of thermal expansion (shown at 0 kPa), there is the added effect of the melting of the crystallites in these regions, which should lead to shape recovery in an unloaded scenario (see appendix H for comparison between curves at constant 600 kPa applied at 60 and 22 °C). Interestingly, in regions III to V, $\varepsilon_{T,2W}$ in the loading direction becomes negative and, instead of elongating with temperature, the sample contracts in the vertical direction. This is due to an increase in the entropy of the system, which is shown to be greater in SMCs than in conventional rubbery elastomers [25]. The opposite happens in the transverse direction, it expands, as expected from the Poisson's effect. This high anisotropy of the $\varepsilon_{T,2W}$ seems to indicate that there is little to no change of volume of the SMC with temperature.

4. Conclusions

The detailed thermo-electro-mechanical characterization of a shape memory composite (SMC) formed by poly(ε-caprolactone) filled with 3 wt% of multiwall carbon nanotubes is investigated during three consecutive one-way shape memory (1W-SM) cycles. Resistive heating is used as means of heating the SMC past the transition temperatures that characterize the shape memory cycles. The resistive heating characteristics of the SMC are a function of its electrical resistivity ρ_e. A PI controller tuned using the lambda method is used to control the temperature of the sample during various mechanical solicitations imparted by a bespoke tensile test bench. This paper presents the detailed evolution of ρ_e through the 1W-SM cycles and its relation with respect to other mechanical and thermo-mechanical properties. The knowledge of these characteristics is helpful in order to better understand the electrically-driven thermally-triggered shape memory cycles of SMCs:

i. The electrical resistivity ρ_e is shown to exhibit a non-linear and non-monotonic dependence during the 1W-SM cycles. Upon heating, ρ_e exhibits a maximum at the melting temperature of the polymer. During the elongation of the sample, ρ_e decreases until a critical strain is reached, after which ρ_e increases. The critical strain is shown to be related to the strain hardening of the sample during elongation. The ρ_e increases during cooling, exhibiting a sudden change when crystallization occurs. During constrained shape recovery the temperature dependence of ρ_e is similar to that of the heating step. During consecutive runs of constrained recovery within the shape memory cycle, good agreement is found in the measured recovery stress. Nevertheless, ρ_e is found to slightly decrease at each constrained shape recovery run.

ii. Similarly to mechanical and shape memory properties, ρ_e also goes through a training process during the first cycle, specifically during its first two steps. The stress-strain curves measured during the loading step of the shape memory cycles show a stiffer behavior of the SMC during the first cycle. After this first training cycle, the SMC turns more ductile.

iii. Despite the above reported variations of resistivity, controlled thermal cycles can be achieved. The presented temperature control loop is extremely efficient in maintaining a constant temperature (temperature stability within ± 0.8 ℃) or a constant sweep rate dT/dt of 10 ℃·min^{-1} due to resistive heating.

Finally, a constant load control is implemented by a fuzzy controller with the purpose of investigating the two-way shape memory (2W-SM) characteristics of the SMC. At a non-zero constant load, the evolution of the 2D strain with temperature is found to be strongly non-linear, due to the stretch-induced crystallization that characterizes 2W-SM semicrystalline composites. The variation on elongation is found to be anisotropic: during heating, the SMC contracts with temperature in the loading direction and elongates in the transverse direction. The opposite occurs with cooling.

The results in this work present the interplay between their electrical, thermal and mechanical properties of SMCs and help identifying the variables that need to be controlled or taken into consideration to achieve repetitive shape memory cycles.

Acknowledgements

References

[1] Chen H, Zhang F, Sun Y, Sun B, Gu B, Leng J and Whang W 2021 *Smart Mater. Struct*. **30** 025040

[2] Liu Y, Zhang F, Leng J, Fu Kun, Lu X L, Wang L, Cotton C, Sun B, Gu B and Chou T W 2019 *Adv. Mater. Technol.* **4** 1900600

[3] Melly S K, Liu Y and Leng J 2020 *J. Mater. Sci.* **55** 10975-11051

[4] Tekay E 2020 *Polymer* **209** 122989

[5] Gong X, Liu L, Liu Y and Leng J 2016 *Smart Mater. Struct.* **25** 035036

[6] He Z, Shi Y, Feng X, Li Z, Zhang Y, Day C, Wang P and Zhao L 2021 *Micromachines* **12** 833

[7] Lei M, Chen Z, Lu H and Yu K 2019 *Nanotechnol. Rev*. **8** 327-351

[8] Leng J, Lan X, Liu Y and Du S 2009 *Smart Mater. Struct*. **18** 074003

[9] Arun D I, Chakravarthy P, Girish B S, Santhosh Kumar K S and Santhosh B 2019 *Smart Mater. Struct.* **28** 055010

[10] Tan Q, Liu L, Liu Y and Leng J 2014 *Compos. Part A Appl.* **64** 132-138

[11] Behl M and Lendlein A 2007 *Soft Matter* **3** 58-67

[12] Zare M, Prabhakaran M P, Parvin N and Ramakrishna S 2019 *Chem. Eng. J.* **374** 706-720

[13] Datta S, Henry T C, Sliozberg Y R, Lawrence B D, Chattopadhyay A and Hall A J 2021 *Polymer* **212** 123158

[14] Tarfaoui M, El Moumen A, Boehle M, Shah O and Lafdi K 2019 *J. Mater. Sci.* **54** 1351-1362

[15] Eisenhaure J and Kim S 2014 *Polymers* **6** 2274-2286

[16] Park J H, Dao T D, Lee H, Jeong H M and Kim B K 2014 *Mater.* **7** 1520-1538

[17] Yenpech N, Intasanta V and Chirachanchai S 2019 *Polymer* **182** 121792

[18] Athanasopoulus N, Baltopoulos A, Vavouliotis A and Kostopoulos V 2012 *Polym. Compos.* **33** 1302-1312

[19] Yu K, Liu Y and Leng J 2011 *J. Intell. Mater. Syst. Struct.* **22** 0369-11

[20] Gu J, Zhao S, Duan H, Wan M and Sun H 2021 *J. Intell. Mater. Syst. Struc*. **00** 1-12

[21] Yang B, Infuence of moinsture in polyurethane shape memory polymers and their electrically conductive composites, Doctoral thesis, Nanyang Technological University, 2007

[22] Pieczyska E A, Staszczak M, Kowalczyk-Gajewska K, Maj M, Golasinski K, Golba S, Tobushi H and Hayashi S 2017 *Polym. Test.* **60** 333-342

[23] Matsui R, Takeda K, Tobushi H and Pieczyska E 2018 *J. Theor. Appl. Mech*. **56** 447-456

[24] Tobushi H, Mitsui K Thermomechanical Properties of Shape Memory Polymer. In: Hetnarski R.b. (eds) Encyclopedia of Thermal Stresses, Springer, Dordrecht, 2014

[25] Chung T, Romo-Uribe A and Mather P T 2008 *Macromol.* **41** 184-192

[26] Posada Murcia A, Uribe Gomez J M, Sommer J U and Ionov L 2021 *Macromol.* **54** 5838-5847

[27] Westbrook K K, Parakh V, Chung T, Mather P T Wang L C, Dunn M l and Jerry Qi H 2010 *J. Eng. Mater. Technol*. **132** 041010

[28] Sanchez-Garcia M D, Lagaron J M and Hoa S V 2010 *Compos. Sci. Techol.* **70** 1095-1105

[29] Naseri A, Diba M, Golkar S, Boccaccini A R, Klupp Taylor R N 2014 *Mater. Lett.* **130** 164-167

[30] Chen Y F, Tan Y J, Li J, H Y B, Shi Y D and Wang M 2018 *Polym. Test.* **65** 387-397

[31] Kang S, Kang T H, Kim B S, Oh J, Park S, Choi S I, Lee J and Son J G 2019 *Compos. B Eng.* **162** 580-588

[32] Defize T, Thomassin J M, Alexandre M, Gilbert B, Riva R and Jérôme C 2016 *Polymers* **84** 234

[33] Pereira Sánchez C, Houbben M, Fagnard J F, Laurent P, Jérôme C, Noels L and Vanderbemden P 2022 *Smart Mater. Struct*. **31** 025003

[34] Aström K J and Murray R M *Feedback Systems: An Introduction for Scientists and Engineers,* Princeton University Press, 2010

[35] Bucz S and Kozáková A 2018, *Advanced Methods of PID Controller Tuning for Specified Performance*. In book: *PID Control for Industrial Processes*, IntechOpen, pp. 73-119

[36] Hambali N, Masngut A, Ishak A A and Janin Z 2014 *IEEE International Conference on Smart Instrumentation, Measurements and Applications (ICSIMA),* pp. 1-6

[37] Seborg D E, Edgar T F and Mellichamp D A *Process Dynamics and Control.* 2nd ed. Hoboken, NJ: John Wiley & Sons, Inc., 2004

[38] Ohki T, Ni Q Q, Ohsako N and Iwamoto M 2004 *Compos. Part A Appl.* **35** 1065-1073

[39] Dachang Z, Baolin D, Puchen Z and Shouyan C 2020 *Complexity* **2020** 3491845

[40] Sun Q, Du C, Duan Y, Ren H and Li H 2021 *Wireless Netw.* **27** 3537-3547

[41] Goh P S, Ismail A F and Ng B C 2014 *Compos. Part A Appl.* **56** 103-126

[42] Ni Q Q, Zhang C, Fu Y, Dai G and Kimura T 2007 *Compos. Struct.* **81** 176-184

[43] Nielsen L E and Landel R F Mechanical Properties of Polymers and Composites, 2nd ed, CRC Press, 1993

[44] Tasis D, Carbon nanotuve-polymer composites, RSC Nanoscience and Nanotechnology, 27, RSC Publishing, Cambridge, 2013

[45] Nie D, Yin X, Cai Z and Wang J 2022 *Polym.* **14**, 1569

[46] Ge Q, Luo X, Rodriguez E D, Zhang X, Mather P T, Dunn M L and Qi H J 2011 *J. Mech. Phys. Solids* **60** 67-83

Appendix A: Properties of MWCNT Nanocyl 7000, data taken from the manufacturer

Table A.1: Characteristics of the MWCNT Nanocyl 7000 used in the shape memory composites (data taken from the manufacturer's datasheet).

Parameter	Value
Average diameter [nm]	9.5
Average length [µm]	1.5
Carbon purity [%]	90
Transition metal oxide [%]	<1
Surface Area [m2·kg-1]	0.25-0.3
Volume resistivity [$\Omega \cdot$ m]	1e-5

Appendix B: Transmission Electron Microscopy (TEM) images of the SMC composed of PCL filled with 3 wt% MWCNT

The quality of the dispersion of the MWCNT inside of the PCL matrix is checked by Transmission Electron Microscopy (TEM). Multiple thin sections of the SMC were prepared and imaged in TEM. An example of the dispersion can be seen in Figure B.1. The MWCNT do not form agglomerates within the material after a mixing time of 60 minutes in the co-rotating twin screw mini-extruder. The MWCNT are also observed to be randomly dispersed, forming some interconnected paths while keeping a random distribution and orientation through the thin layer of SMC. Considering the high amount of filler content used during this investigation (3 wt% MWCNT) and the absence of agglomerates, we consider the dispersion to be homogeneous enough for the purpose of the investigation reported in this article.
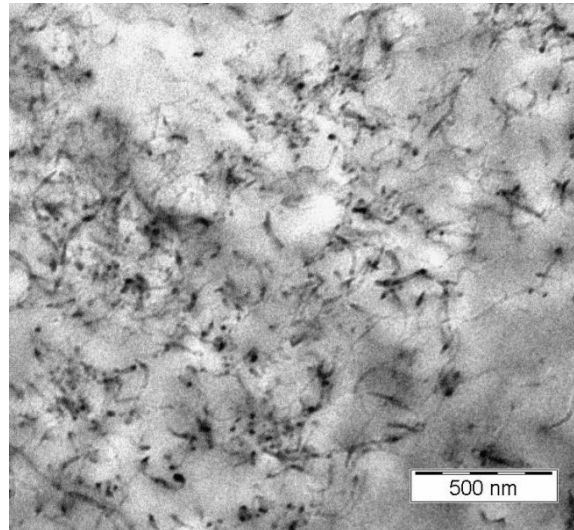
Figure B.1: Image of the distribution of MWCNT within the shape memory polymer matrix obtained from Transmission Electron Microscopy (TEM) of the SMC composed by PCL filled with 3 wt% MWCNT.

Appendix C: Preliminary electrical and electro-mechanical characterization of PCL with different concentrations of MWCNT.

Several concentrations of MWCNT were dispersed inside of the PCL shape memory polymer. The electrical resistivity of the resulting SMC samples is measured in a four-point configuration by injecting a small electric current (< 1 mA) for which no measurable resistive heating arises. The electrical resistivity of the SMC is hence that at room temperature. Figure C.1 shows a box and whiskers plot of the electrical resistivity of the resulting composite for MWCNT concentrations ranging from 1 to 5 wt%. The median electrical resistivity $\widetilde{\rho_e}$ of each MWCNT content group is represented by a horizontal red line, and the values are also reported in the figure. The few outliers, represented by red + signs, are also shown.
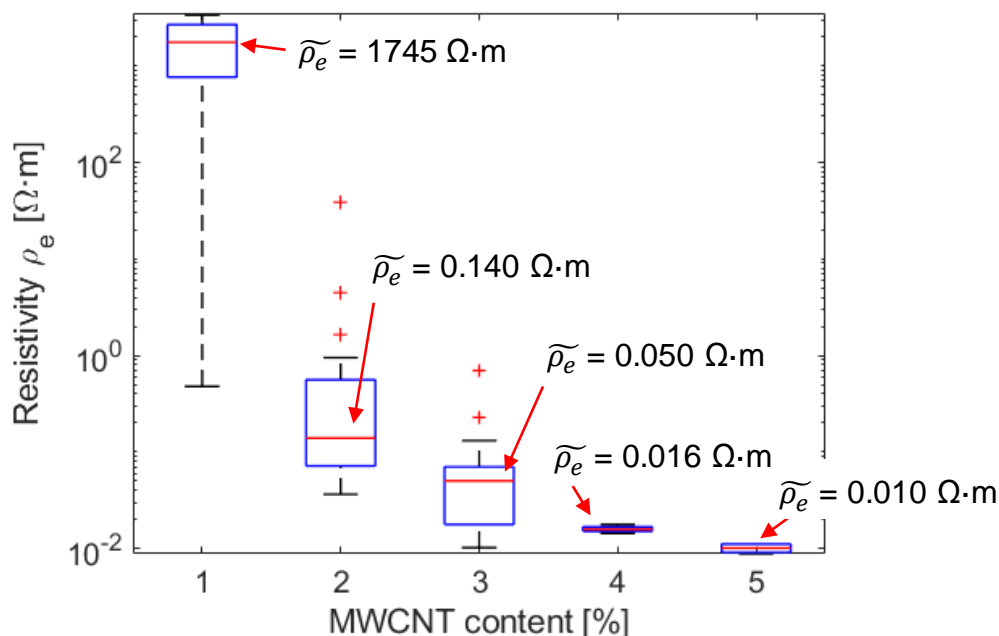

Figure C.1: Box and whiskers plot of the electrical resistivity of PCL with different contents of MWCNT. Red "+" signs denote outliers. The red horizontal lines denote the median resistivity $\widetilde{\rho_e}$ of the measured samples.

Figure C.1 shows that, at each individual filler concentration, there is a statistical dispersion of the measured electrical resistivity from sample to sample due to unavoidable local variations in the dispersion of MWCNTs. This explains the difference in the resistivity values between those reported in the main body of the article and those reported in the appendices. The electrical resistivity of pristine PCL is in the order of 10^{11} $\Omega \cdot$m [44]. The measured electrical resistivity of SMC with 1 wt% MWCNT is in the order 10^0 to 10^3 $\Omega \cdot$m, more than 8 orders of magnitude smaller. Thus, it can be considered that the percolation threshold for this SMC is already surpassed for MWCNT concentrations equal to 1 wt%. Nevertheless, there is a great variation in the measured values of samples with the same composition.

For higher concentrations of 2 wt% MWCNT the median resistivity of the tested samples decreases to 0.14 $\Omega \cdot$m, which facilitates the increase of temperature due to the injection of an electric current. Furthermore, the variation of electrical resistivity among different samples of the same composition is much smaller than for 1 wt% MWCNT, which may lead to more reproducible resistive heating. The same trend can be seen for higher concentrations of MWCNTs: decreased value of the median and lower variation among tested samples.

To justify the choice made in the current investigation of PCL filled with 3 wt% MWCNT, the electrical resistivity evolution with strain in Figure C.2 is investigated. The reported Green-Lagrange (GL) strain is a result of a uniaxial tensile test performed at 65 °C and at a deformation rate of 0.02 mm·s^{-1}. The experimental conditions are similar to those reported in the main body of the article. The measured evolution of electrical resistivity is shown for two samples in different line textures for each MWCNT content. As it can be seen, the measured evolution of the electrical resistivity with GL strain for PCL with 2 wt% MWCNT grows by an average of 80% from the original state at no deformation to a strain of 1 mm·mm^{-1}. Nevertheless, the average growth for the SMC with 3 wt% MWCNT is only of 39%. The lower variation in electrical resistivity with strain in the loading direction is expected to enhance the reproducibility of the results during the shape memory cycles. Moreover, the lower overall value of electrical resistivity at large deformations ensures an adequate resistive heating during the complete shape memory cycle. For the sake of scientific rigor, we should mention that the composite in this Figure C.2 was made with a commercially-available PCL that unfortunately was later discontinued. This commercially-available PCL has a molecular weight of 9600 g·mol^{-1} (PCL76-4arms, 19 units per arm). Since then, a PCL synthesized in-house with the same 4-arm morphology and very close molecular weight was prepared and used for all other investigations reported in this manuscript. The newly synthesized PCL used as a polymer matrix of the SMC shown in the rest of the figures has a molecular weight of

10300 g·mol^{-1} (PCL82-4arms, 20.5 caprolactone units per arm). This corresponds to 1.5 more caprolactone units per arm (in average) as compared to the old one. This slight variation in the PCL composition has no measurable impact on the viscosity of the mix during the preparation of the composite. The functionalisation of the PCL stars is not impacted either. Furthermore, the differences between the thermo-mechanical and electrical properties measured with both PCL networks fall within statistical errors.
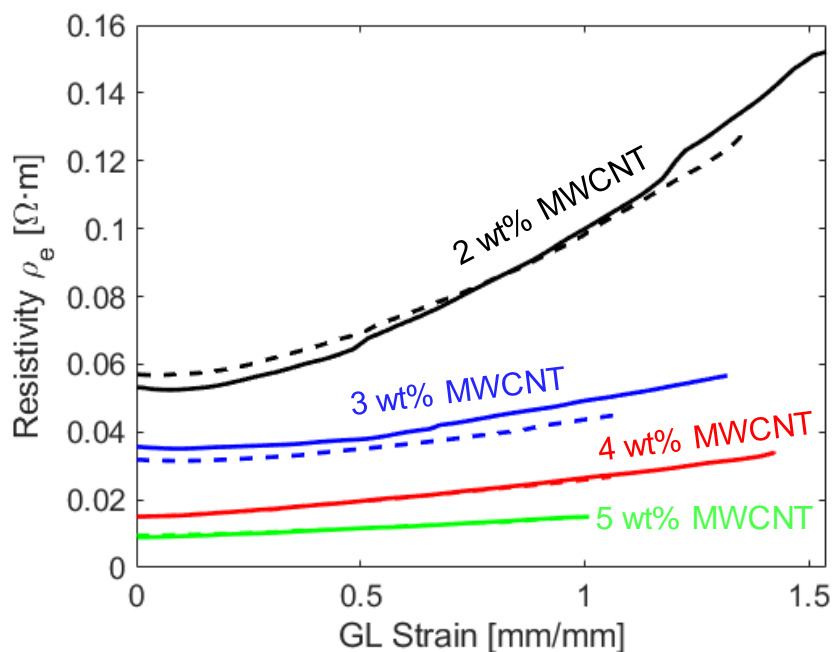

Figure C.2: Green-Lagrange (GL) strain dependence of the electrical resistivity of the SMC samples with different contents of MWCNTs. The GL strain is a result of a uniaxial tensile test performed at 60 °C and at a constant deformation rate of 0.02 mm·s^{-1}. Different line textures denote different samples of the same composition.

Appendix D: Results obtained by Differential Scanning Calorimetry (DSC) on the SMC between 25 and 65 °C with temperature ramps of 10 °C·min^{-1}
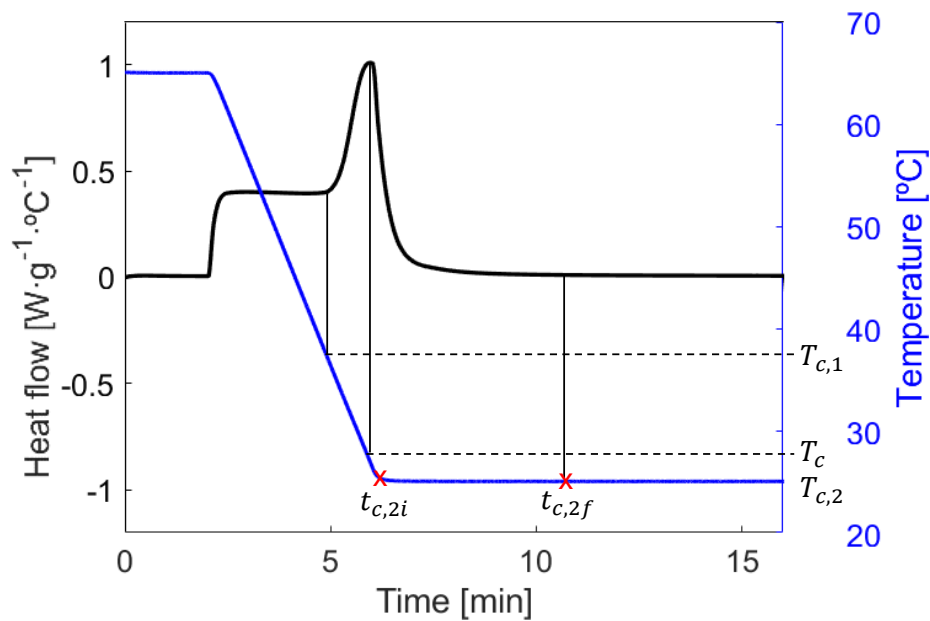
The heat flow evolution with temperature is measured in Differential Scanning Calorimetry during a heating cycle that mimics the experimental conditions for resistive heating reported in the main body of the article. First, the material is heated to 65 °C. The temperature cycle specified in DSC starts by maintaining the sample at 65 °C for 5 minutes in order to eliminate any thermal history. Then, the sample is cooled down from 65 to 25 °C, leaving it for 10 minutes at 25 °C. The sample then gets heated up to 65 °C once again. The heating and cooling ramps are set to ±10·°C·min^{-1}. The heat flow evolution during this cycle is shown in Figure D.1.
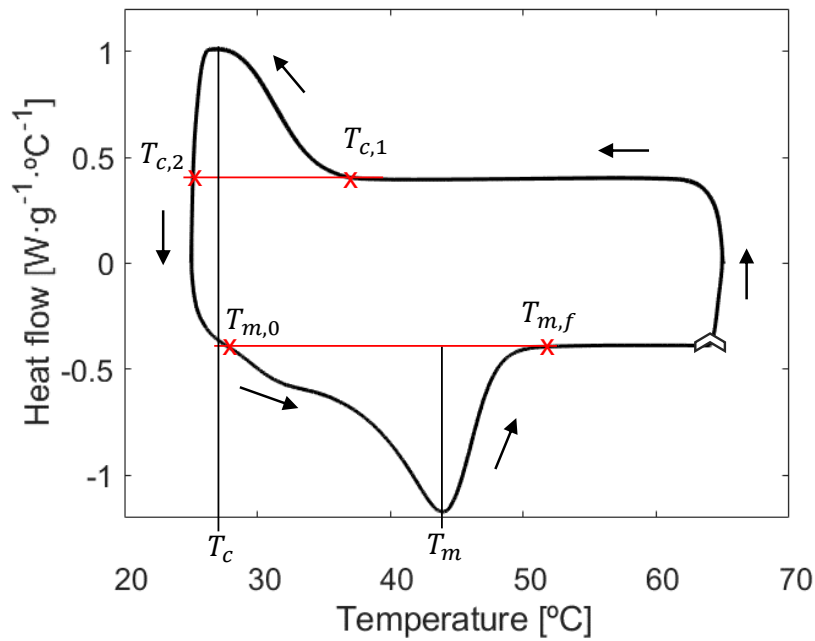
Figure D.1: Heat flow evolution with temperature measured in Differential Scanning Calorimetry (DSC) on the SMC under study. The starting point of the temperature cycle is shown with a chevron. The direction of the temperature cycle is indicated in black arrows. The temperature cycle ranges from 25 to 65 °C with temperature ramps at 10 °C·min^{-1}. The characteristic temperatures of melting and crystallization (with the starting and ending points) are marked by red crosses.

As can be seen from the heat flow evolution with temperature, the melting process starts at $T_{m,0}$ = 28.6 °C and finishes at $T_{m,f}$ = 52.7 °C with a peak melting temperature T_m = 43 °C. During cooling at -10 °C·min^{-1}, the crystallization is shown to start at $T_{c,1}$ = 36.9 °C and to finish at the lowest temperature of $T_{c,2}$ = 25 °C. The exothermic crystallization peak lies at T_c = 26.6 °C.

Even though the crystallization ends at 25 °C, it does not do so as soon as the material reaches said temperature. Figure D.2 shows the heat flow and the temperature evolution with time during the cooling part of the cycle. The temperature reaches 25 °C at a time $t_{c,2i}$. At this time, the heat flow is still non-zero and keeps decreasing with time, which indicates that crystallization has not finished yet. The heat flow reaches zero at a time $t_{c,2f}$. The difference in time from $t_{c,2f}$ and $t_{c,2i}$, i.e. 5.1 minutes, is the time needed for crystallization to finish during the isotherm at 25 °C. During the resistive heating experiments presented in the main body of the article, the SMC is always left during 10 minutes at room temperature in order to ensure full crystallization of the material.

Figure D.2: Heat flow (in black, to be read on the primary *y*-axis) and temperature (in blue, to be read on the secondary *y*-axis) evolution with time during crystallization of the SMC sample from 65 to 25 °C at -10 °C·min^{-1}. The crystallization temperatures and times are marked.

Appendix E: Result of the PI controller tuned using the lambda tuning method to obtain a desired thermal profile and resulting injected current to obtain said temperature.

Conventionally, when heating a SMC electrically, a constant voltage (or current) is applied onto the sample to achieve a certain temperature increase. By applying a voltage V, the power dissipated by resistive heating would be $\frac{V^2 L}{\rho_e we}$, where L, w and e are the length, width and thickness of the sample respectively. As evidenced by the results displayed in the main body of this article, the resistivity of a SMC specimen varies depending on (i) temperature, (ii) deformation or (iii) number of shape memory cycles. If a constant voltage (or current) is applied, the are several implications, possibly deleterious, to consider:

(1) The temperature increase due to a voltage (or current) step (or temperature decrease due to turning off the voltage source) will not be linear but it will follow a $1 - \exp(-t/\tau)$ law until the steady-state temperature is reached [5]. The variation of the electrical resistivity with the above-mentioned parameters makes the prediction of the required voltage (or current) to obtain a linear temperature very intricate.

(2) As shown in Figure 4(b) of the main body of the article, the resistivity increases with strain for high values of strain (values above the defined critical strain ε_c marked with crosses). Thus, for a constant applied voltage, the temperature on the SMC would decrease. If the temperature decreases to values where crystallization starts occurring, the SMC can fix the temporary shape, which further increases the resistivity, as shown in Figure 4(c). If the deformation is not stopped even though crystallites are present in the network, considerable damage can be made onto the SMC sample. A possibility to avoid this scenario would be to apply a much higher voltage than necessary. However, besides not being energy-efficient, the SMC under consideration can uncrosslink at high temperatures (around 120 °C) due to the Diels-Alder reaction.

(3) The steady-state temperature reached when applying a constant voltage would be dependent on the number of shape memory cycles previously performed. Additionally, it is likely to change depending on the surroundings, such as variations in room temperature, gusts of air, etc. These would also influence the heating and cooling ramps. In semi-crystalline SMCs; cooling is an important part of a thermal cycle to control since the size and quantity of the crystalline regions depend on the cooling rate, i.e. a higher cooling rate induces lower crystallinity degree [45]. These crystalline regions fix the temporary shapes of the SMC and hence are directly related to the shape fixity [46] and shape recovery of the material [25, 45]. It has been reported that high temperature ramps are related to lower shape fixity and higher shape recovery. Applying a constant voltage in this scenario would result in an uncontrolled crystallization and, hence, in less repetitive shape memory characteristics.

(4) Different samples of SMC have different electrical resistivities. Applying a constant voltage to all samples would result in very different thermal cycles from sample to sample, possibly not even being able to surpass the melting temperature required for inducing any shape change.

The investigation carried out in our work overcomes these drawbacks by using a temperature controller of resistive heating instead of the conventionally applied constant voltage (or current). As it is explained in section 2.5 of the main body of the article, a PI controller is used in order to control the measured average temperature on the surface of the SMC that is a result of resistive heating. The temperature control of resistive heating has, to our knowledge, not been reported in the literature. Figure E.1 shows the resulting thermal cycle previously introduced in section 2.5. The time evolution of the injected current, whose value is calculated by the PI controller, is also shown together with the measured resistivity of a SMC sample. The absolute values reported in this graph for a SMC with 3 wt% MWCNT at zero strain differ from the corresponding values reported in Figure 4 (a) in the main body of the article. This is due to the unavoidable statistical distribution of the resistivity at zero strain from sample to sample. This is quantified in our samples and reported in the box and whiskers plot of Appendix C (Figure C.1). As expected from the non-monotonic evolution of the electrical resistivity with to temperature, the calculated current resulting from the PI control does not increase linearly during the heating and cooling ramps. It has been shown in the results of Figure 2, 4 and 6 that a PI controller tuned with the lambda method achieves a very favourable temperature control throughout shape memory cycles. Several SMC samples with different resistivities have been used with similarly successful results.
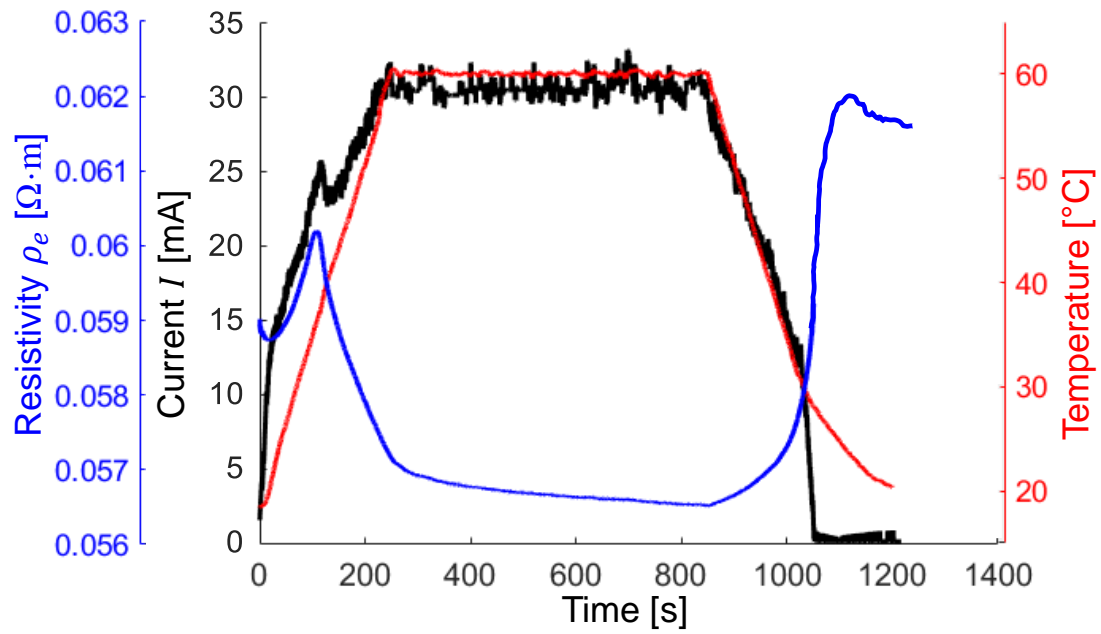
Figure E.1: Time evolution of the controlled temperature (in red) measured as the average on the surface of a SMC sample. The temperature control is achieved using the lambda tuning method explained in section 2.5 of the main body of the article. The evolution of the injected current with time in order to obtain said temperature is shown in black. The measured resistivity of the SMC is also shown in blue as a function of time.

Appendix F: Details on fuzzy logic controlled used for constant load control of the tensile test bench during thermal expansion/contraction of the SMC

The designed fuzzy controller is based on the load error (LE, difference between the measured load and the constant load setpoint) used as an input variable. The controller calculates then the corresponding actuator linear velocity (AV). Both the input and output membership functions of the controller are Λ-type and the corresponding fuzzification rules are described in Figure F1. When the CTE is measured well above or well below the transition temperature, the expansion/contraction is small and therefore small adjustments on the position of the grip will be needed. However, in order for the load not to quickly diverge from the constant setpoint around the transition temperature, where most of the expansion/contraction occurs, the (Very) High/Low membership functions are set in order to cause the (Very) Fast Down/Up output respectively. The No Motion output membership function is defined by the minimum speed of the actuator system.
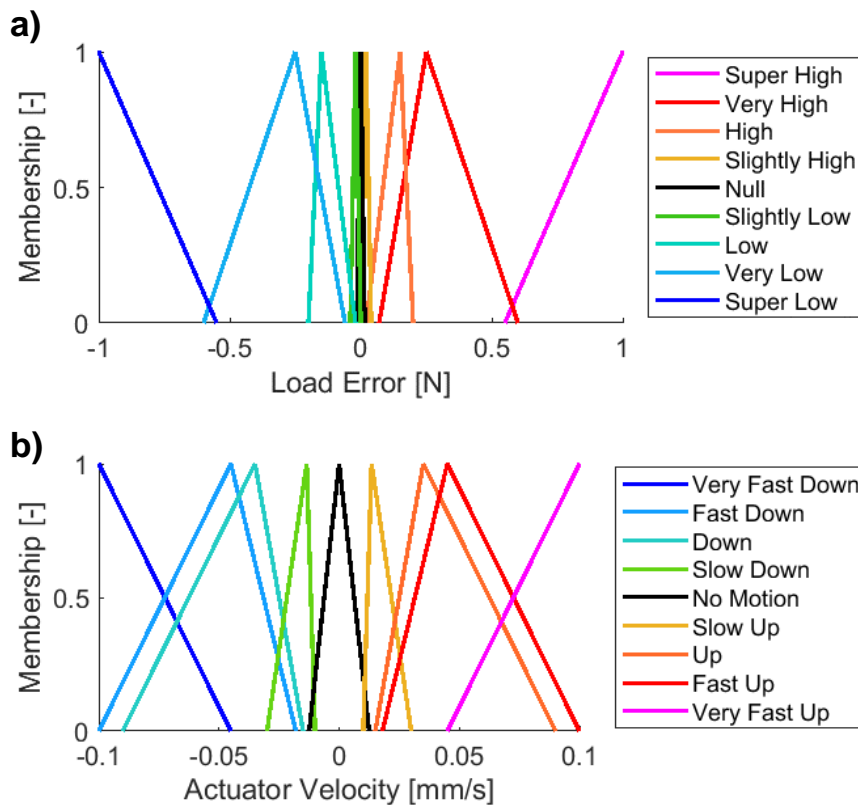
Figure F.2: Membership functions for (a) the input load error and (b) the actuator vertical velocity of the fuzzy controller.

The fuzzification rules read as follows:
i)   If LE is Super Low then AV is Very Fast Down.
ii)   If LE is Very Low then AV is Fast Down.
iii) If LE is Low then AV is Down.
iv)   If LE is Slightly Low then AV is Slow Down.
v)   If LE is Null then AV is No Motion.
vi)   If LE is Slightly High then AV is Slow Up.
vii) If LE is High then AV is Up
viii) If LE is Very High then AV is Fast Up
ix)   If LE is Super High then AV is Very Fast Up.
The defuzzification method is center of area.

Appendix G: Electrical resistivity and recovery stress evolution during cycles 2 and 3 of Constrained shape recovery.

The temperature dependence of the electrical resistivity ρ_e during the cycles 2 and 3 of Constrained shape recovery can be seen in solid lines in Figure G1. The three performed runs of Constrained shape recovery are shown for each cycle. Figure G1(a) and (b) show the Constrained heating and cooling for cycle 2. Figure G1(c) and (d) show the Constrained heating and cooling for cycle 3. The evolution of ρ_e with temperature for each run is similar to the one reported in the main body of the article for cycle 1 (see Figure 5). The mean value of ρ_e increases with each cycle, as expected from the results shown in Figure 4(d) of the main body of the article.
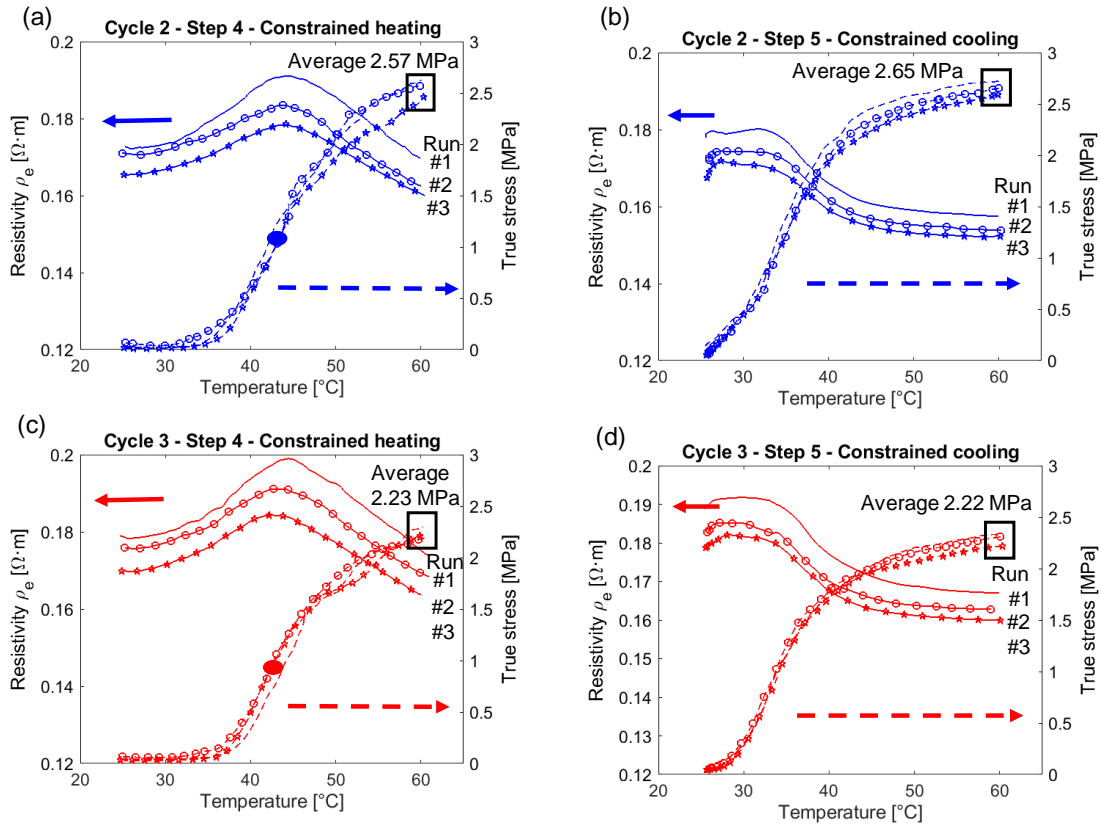

Figure G.1: Temperature dependence of the resistivity and stress measured during (a) Cycle 2 – Constrained heating, (b) Cycle 2 – Constrained cooling, (c) Cycle 3 – Constrained heating and (d) Cycle 3 – Constrained cooling. For each of them, the three consecutive runs are shown: run 1 (no marker), run 2 (circles) and run 3 (stars). Solid lines are used for resistivity and should be read on the left *y*-axis. Dashed lines are used for the stress and should be read on the right *y*-axis. The solid dot in (a) and (c) marks the inflexion point of the recovery stress vs. temperature. Grey vertical dashed lines mark the melting temperature in (a) and (c) and the temperature at the start of crystallization in (b) and (d).

The (true) recovery stress σ_R, shown in Figure G1 in dashed lines (to be read on the right *y*-axis) in each of the four subplots, show similar increase/decrease behavior with temperature for the heating/cooling step. The final value of σ_R obtained during Constrained heating at 60 °C (or the first value at the same temperature during Constrained cooling) is shown to decrease with each shape memory cycle. The average value of σ_R among the three Constrained shape recovery runs is reported in Table 1 of the main body of the article for each of the three shape memory test cycles. The decrease of σ_R with each shape memory test cycle can be anticipated when looking at Figure 7 of the main body of the article: a lower stress is applied each cycle on the sample in order to achieve the specified elongation because of the softening of the material.

Appendix H: Extra information on the evolution of the (surface) average GL strain with temperature at constant stress during heating and cooling for the investigation of the two-way shape memory (2W-SM) effect.

The strain measured on the sample during heating and cooling at constant pre-stress, is shown as a function of the temperature in Figure H1. The pre-stress is pre-applied at 60 °C in a previous temperature cycle (see section 2.7.3 in the main body of the article). The strain in the loading and transverse directions (y and x-axis respectively) at two pre-stress levels of 0 and 600 kPa are shown. The five regions specified in the main body of the article are based on the melting temperature T_m of the SMC and the CTE estimated during the heating part of the temperature cycle at no load in each of these regions is already reported in Table 2. Similar temperature regions are defined with respect to cooling based on the temperature at the start of crystallization $T_{c,1}$ and these are shown in Figure H1. The temperature regions are defined as:

(VI) $T > T_{c,1} + 2$; (VII) $T_{c,1} + 2 > T > T_{c,1} - 2$; (VIII) $T_{c,1} - 2 > T$.
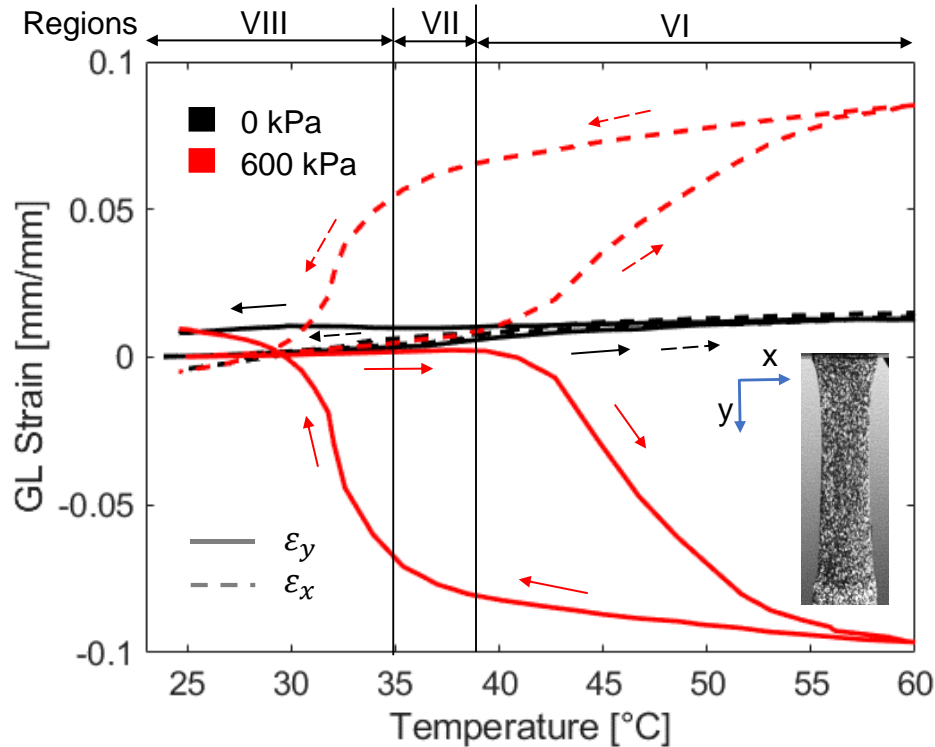
Figure H.1: Evolution of GL strain with temperature at constant stress for the investigation of the two-way shape memory (2W-SM) effect. Two constant pre-stress levels are shown: 0 kPa (in black) and 600 kPa (in red). The strain in the x-direction (transverse direction) is shown by dashed lines and the strain in the y-direction (loading direction) is shown by solid lines. Small (black or red) arrows specify the direction of the temperature loop. Three regions are identified for the calculation of the CTE (at 0 kPa) during cooling.

The corresponding CTEx and CTEy calculated during cooling part of the curves at 0 kPa in each of these regions are reported in Table H.1. The estimated values are always at the same order of magnitude of 10^{-3} °C^{-1} as as during the heating curve.

Table H.1: Estimation of the linear Coefficient of Thermal Expansion at zero stress during cooling in the loading and transverse direction (CTEy and CTEx respectively) in the three temperature regions specified in Figure H1.

Region	VIII	VII	VI
CTEx [10^{-3} °C^{-1}]	0.2	0.4	1.0
CTEy [10^{-3} °C^{-1}]	0.1	< 0.1	0.4

The evolution of strain with temperature due to the 2W-SM effect ($\varepsilon_{T,2W}$) at 600 kPa is still negative during cooling in the loading direction. Most of the deformation during cooling happens in region VIII, which is, most probably, where most of the crystallization happens. Furthermore, one can see that the strain in the loading direction (y-direction) at the end of cooling is higher than zero (the starting point). This is expected since, if one recalls Figure 5 (in the main body of the article) or Figure G1, the recovery stress decreases with consecutive temperature cyclings at constant strain. Therefore, in this case at constant stress, the sample would need to have a higher elongation in order to maintain said constant stress. Nevertheless, this final value of the strain needed to maintain a constant stress of either 0 or 600 kPa is very small (< 0.01 mm·mm^{-1}).

In order to observe how the shape memory properties of the SMC affect the thermal expansion, a similar sample was used to measure the GL strain upon a heating and cooling cycle at a constant pre-stress of 600 kPa. In this case, the pre-stress was first applied at 60 °C (as done previously) and maintained while cooling down to room temperature. Then, the cycle to investigate the 2W-SM properties was performed. After finishing performing the measurement, the sample was unloaded at 60 °C, cooled down to room temperature and left for 10 min to crystallize. A similar measurement was then performed but this time applying the pre-stress at 22 °C (room temperature. The GL strain measurement starts after 10 min of isostress at room temperature. The variation of the GL strain upon the heating and cooling ramps for both cases are shown in Figure H2 in red and blue respectively. The strain in the loading (*x*-) and transverse (*y*-) directions are shown by solid and dashed lines respectively.
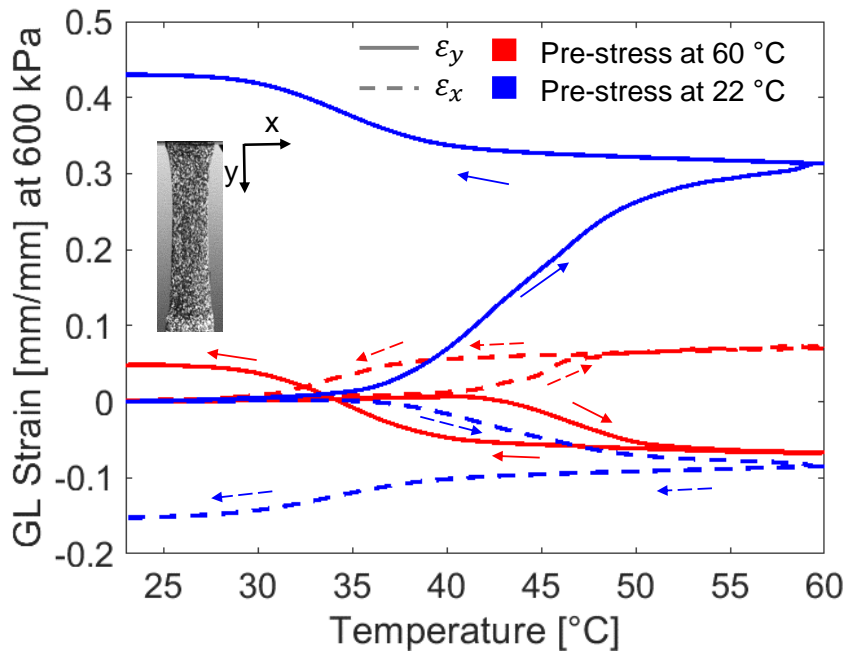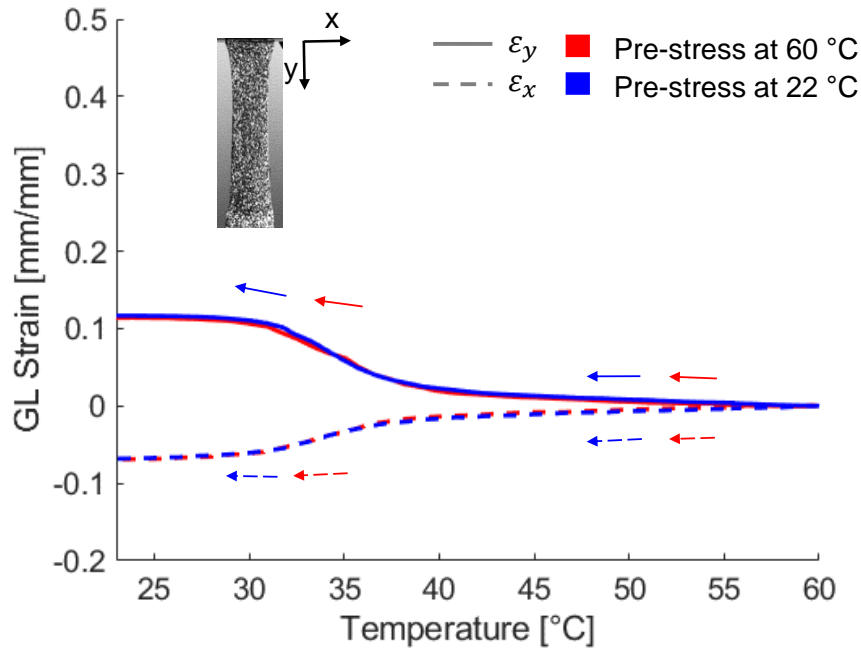

Figure H.2: Evolution of GL strain with temperature of a sample under at constant pre-stress equal to 600 kPa. The pre-stress is applied at a constant temperature of 22 °C (in blue) and 60 °C (in red). In latter case, the sample is cooled down to room temperature (22 °C) before performing the temperature cycle shown. The strain in the *x*-direction (transverse direction) is shown by dashed lines and the strain in the *y*-direction (loading direction) is shown by solid lines. Small (red or blue) arrows specify the direction of the temperature loop.

As can be seen, when the pre-stress is applied at room temperature (blue curve), the strain in the loading direction increases with temperature during heating, while a contraction is seen in the transverse direction. Similar to what was observed in Figure 8, most of the deformation still happens around the peak melting temperature of the SMC. However, the absolute value of the deformation attained in this case during heating is higher than in the case where the pre-stress was applied at 60 °C. This difference amounts to 370% in the loading direction and 0.16% in the transverse direction. The significant difference in the loading direction appears because (i) the SMC is much softer after melting and, in order to maintain a constant stress, the sample pre-stressed at 22 °C needs to be elongated further during the phase change; and (ii) the pre-stressed sample at 60 °C has already experienced the elongation required to compensate for the low stiffness of the material once past the melting during the application of the pre-stress. Nevertheless, the anisotropy of the strain is maintained (elongation in the loading direction while contraction on the transverse). The contraction seen in the transverse direction for the sample pre-stressed at 22 °C is a result of the Poissons' ratio, i.e. the cross-section of the sample is reduced with the elongation required to maintain constant stress. Coincidentally, the value of the ratio $-\varepsilon_x/\varepsilon_y$ of the blue curve at the end of the heating ramp amounts to 0.26.

During cooling, however, the expansion/contraction in the loading/transverse direction of the sample pre-stressed at 22 °C recovers the same behavior seen when pre-stressed at 60 °C, i.e. a negative $\varepsilon_{T,2W}$. This is expected since, once molten, the sample pre-stressed at 22 °C has virtually the same thermomechanical history than the sample pre-stressed at 60 °C, except for potential (but visibly minimal) damage due to the elongation at room temperature. In order to illustrate this, Figure H3 shows the same GL strain curves of Figure H2 but only during the cooling ramp (subtracting the value of the strain at 60 °C to each curve). It can be seen that the agreement of the $\varepsilon_{T,2W}$ during the cooling ramp is remarkably similar for both pre-stressed cases. Most of the elongation happens, once again, around the crystallization temperature of the SMC.

Figure H.3: Evolution of GL strain with temperature during cooling of a sample under at constant pre-stress equal to 600 kPa. The pre-stress is applied at a constant temperature of 22 °C (in blue) and 60 °C (in red). In the latter case, the sample is cooled down to room temperature (22 °C). Both samples are then heated to 60 °C in order for the cooling curve shown to start. The strain in the *x*-direction (transverse direction) is shown by dashed lines and the strain in the *y*-direction (loading direction) is shown by solid lines. Small (red or blue) arrows specify the direction of the temperature loop.

The data provided in this appendix gives evidence that the evolution of strain with temperature typical of the 2W-SM effect is anisotropic in the loading and transverse directions. The characteristics of the SMC and the thermomechanical history of the sample play an important role on the elongation/contraction of the sample upon a temperature ramp that crosses phase changes, i.e. melting or crystallization.